How a reaction-diffusion signal can control spinal cord regeneration in axolotls: A modelling study

Valeria Caliaro[1], Diane Peurichard[1], and Osvaldo Chara[2,3,*]

[1]Inria Paris, team MAMBA, Sorbonne Université, CNRS, Université de Paris, Laboratoire Jacques-Louis Lions UMR7598, F-75005 Paris, France
[2]School of Biosciences, University of Nottingham, Sutton Bonington Campus, Nottingham LE12 5RD, UK
[3]Instituto de Tecnología, Universidad Argentina de la Empresa, Buenos Aires C1073AAO, Argentina
[*]Corresponding author. Email : osvaldo.chara@nottingham.ac.uk

August 21, 2023

Abstract

Axolotls are uniquely able to completely regenerate the spinal cord after amputation. The underlying governing mechanisms of this regenerative response have not yet been fully elucidated. We previously found that spinal cord regeneration is mainly driven by cell cycle acceleration of ependymal cells, recruited by a hypothetical signal propagating from the injury. However, the nature of the signal and its propagation remain unknown. In this theoretical study, we investigated whether the regeneration-inducing signal can follow a reaction-diffusion process. We developed a computational model, validated it with experimental data and showed that the signal dynamics can be understood in terms of reaction-diffusion mechanism. By developing a theory of the regenerating outgrowth in the limit of fast reaction-diffusion, we demonstrate that control of regenerative response solely relies on cell-to-signal sensitivity and the signal reaction-diffusion characteristic length. This study lays foundations for further identification of the signal controlling regeneration of the spinal cord.

1 Introduction

In contrast to most vertebrates, salamanders are capable of remarkable regeneration traits. Although more than 250 years have passed since the original discovery of salamander tail regeneration after amputation by Spallanzani [1], the governing mechanisms underlying these unparalleled regeneration capabilities have not yet been completely elucidated. The axolotl (*Ambystoma mexicanum*) is a paedomorphic salamander which can resolve severe and extreme injuries of the spinal cord throughout complete and faithful regeneration [2, 3, 4].

Tail amputation in the axolotl triggers the reactivation of a developmental-like program in the ependymal cells, neural stem cells lining in the central canal of the spinal cord [5]. Although cell influx, cell rearrangements, and re-entrance to the cell cycle from quiescence can be observed, the main driver of the spinal cord outgrowth is the acceleration of the cell cycle

[6]. Indeed, during regeneration, ependymal cells anterior to the amputation plane shorten their cycle length three times [5]. We previously identified a high-proliferation zone emerging 4 days after amputation within the 800 μm anterior to the amputation plane that shifts posteriorly during spinal cord regeneration [6]. This particular spatiotemporal pattern was quantified with a recruitment limit curve separating the high-proliferation from the low-proliferation zones [6]. We recently developed the first 1D cell-based computational model of the axolotl spinal cord in which each ependymal cell was simulated with an internal clock portraying its age/position along its cell cycle [7]. The model assumed that tail amputation triggers a hypothetical signal that propagates anteriorly with constant velocity for a certain time along the spinal cord, supposedly one-dimensional, recruiting ependymal cells when the signal concentration is higher than zero. By adapting the Fluorescent Ubiquitination-based Cell Cycle Indicator (FUCCI) technology to axolotls (AxFUCCI), we were able to visualize cell cycles *in vivo*, qualitatively reproducing the model predicted distribution of ependymal cells in coordinates of time, space and cell cycle [7]. Nevertheless, the signal and its nature remain to be elucidated.

Numerous signalling pathways control morphogenetic processes whose dynamics operate under a reaction-diffusion mechanism during development [8, 9, 10, 11] and regeneration [12, 13]. A very well-known example consists of one morphogenetic signal propagating through the tissue while being subjected to an enzymatic degradation or cellular uptake / elimination [14]. This last process constitutes the "reaction" responsible for the consumption of the signal and the consequent reduction in signal concentration. In this study, we aim to determine whether this mechanism could explain the regenerative response observed in the axolotl spinal cord by following a modelling approach combining computational modelling with theory.

To that aim, we here propose a hybrid multi-scale cell-based computational model of the axolotl spinal cord combining the ependymal cell layer with a signal that follows a reaction-diffusion scheme while orchestrating the regenerative response by accelerating the ependymal cell cycle. The model successfully fits the aforementioned recruitment limit curve [6] and correctly predicts the spinal cord outgrowth [5], providing a first estimate of the diffusion coefficient and half-life of the hypothetical regeneration-inducing signal. By using a subsequent rigorous theoretical approach, we finally prove that the spinal cord growth emerging during regeneration in the axolotl can be controlled by the reaction-diffusion characteristic length and the ependymal cell-to-signal sensitivity. Ultimately, this study provides insights into the biophysical properties of signalling processes responsible for successful axolotl spinal cord regeneration.

2 Results

2.1 Hybrid multi-scale model of the ependymal tube controlled by a reaction-diffusion signal qualitatively reproduces spinal cord regeneration in the axolotl

To assess whether spinal cord regeneration in the axolotl can be explained by a potential signaling mechanism operating under a reaction-diffusion scheme, we developed a computational model of the regenerating spinal cord where the ependymal cell division rate is under the control of a generic signal. Specifically, we proposed a multi-scale and hybrid model: while the ependymal cells are featured as non-overlapping and proliferating rigid discs in a "cellular" scale, the density of the signal controlling the ependymal cells is represented by a continuous field in the "signaling" scale (Fig. 1 A, B).

We assumed a 2D domain for both scales, where the two spatial dimensions correspond to

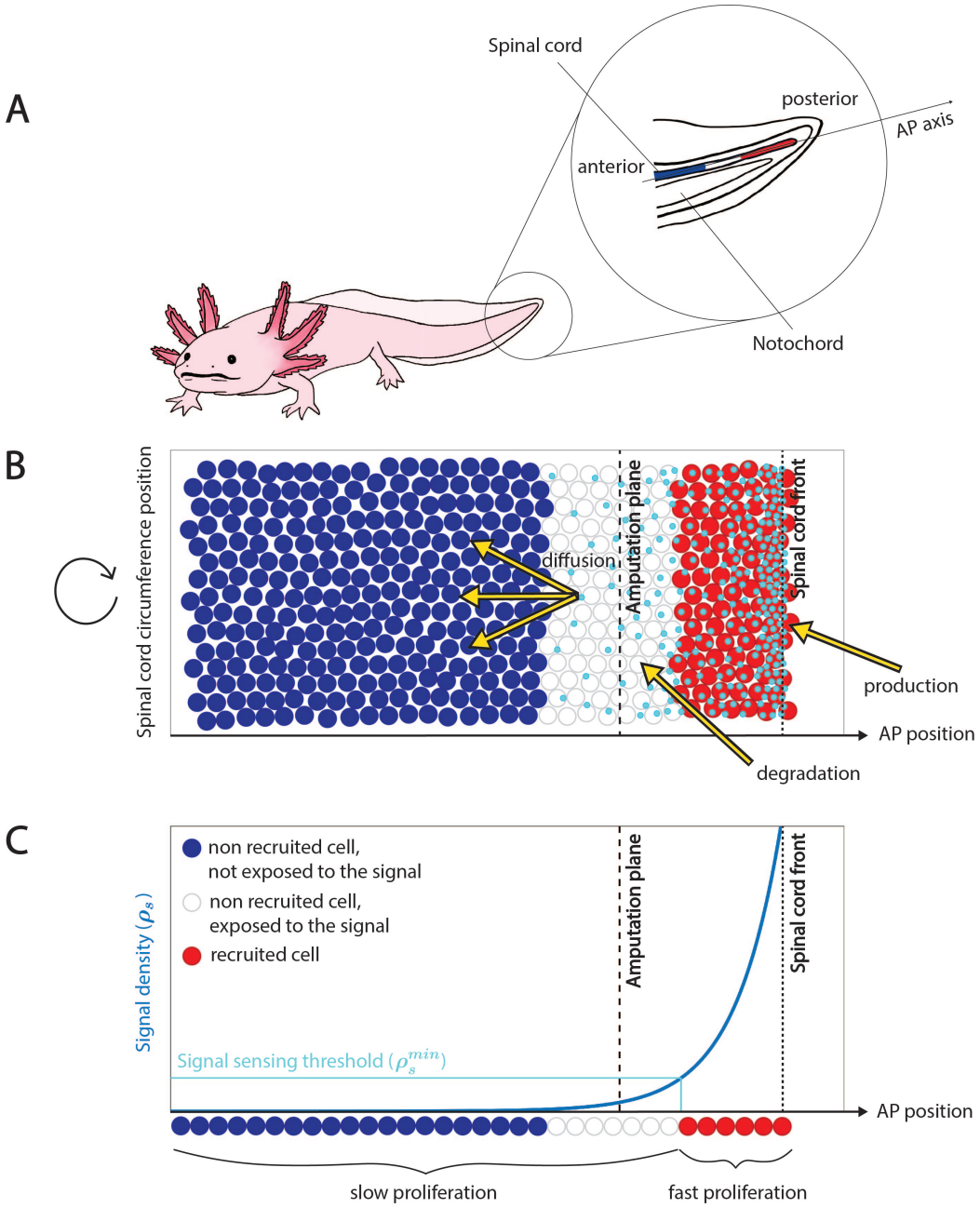

Figure 1: **Schematic representation of the computational model of the signal-dependent regeneration of axolotl spinal cord. (A)** Sketch of the axolotl showing the regenerating spinal cord in the tail. **(B)** Scheme of the model components. The y-axis represents position along the spinal cord circumference and the x-axis corresponds to the Anterior-Posterior axis. The ependymal cells are represented as discs coloured with a French flag-like code, depending on whether they are not exposed to the signal and are not recruited (blue), or they are exposed to the signal but are not recruited (white), or they are exposed to the signal and are recruited (red). The signal is represented as cyan particles that are produced at the front of the tissue, have a finite half-life (degradation) and diffuse in the domain populated by ependymal cells. **(C)** Cell recruitment depends on the local signal density (whose density is here represented in a 1D view). A cell is recruited when it is exposed to a signal density that overcomes the threshold ρ_s^{min} (indicated in cyan). The x-axis represents the AP axis, the blue curve is the density of the signal. In (B) and (C), the amputation plane is indicated by a dashed black line and the spinal cord front is indicated by a dotted black line.

the Anterior-Posterior (AP) axis and the perpendicular direction given by the arc length along the circumference of the central canal apical surface (Circumference axis, Figure 1. A). We modeled the reaction-diffusion mechanism for the signal by assuming that the signal density $\rho_s(x,t)$ linearly degrades with a degradation rate k (which is inversely proportional to the half-life τ) and diffuses with diffusion coefficient D in the domain occupied by the ependymal cells. Mathematically, this can be summarized as follows:

$$\partial_t \rho_S = D\Delta\rho_S - k\rho_S, \tag{1}$$

where the signal density is assumed equal to a non-zero constant at the posterior front of the spinal cord, at any given time t, modeling the secretory signalling centre of the wound epidermis (see details of the boundary conditions for both scales in Supplementary section 2.1). We numerically solved the signaling dynamics by using the Smoothed-Particle Hydrodynamics (SPH) method [15] which approximates the density function $\rho_S(x,t)$ by a cloud of N "signalling" particles of equal and constant masses, convected along their regularized concentration gradient following the diffusion velocity method [16] (see justification of this method as well as details on the numerical implementation in the Supplementary section 2.2).

Based on our previous study [7], we assumed that in the absence of the signal, the ependymal cells progress along their cell cycle with a certain pace (essentially, the cell cycle length is supposed lognormally distributed and the initial position of the cells within the cell cycle follows an exponential distribution; for more details of the stochastic component of the model, see [7]). Cells exposure to a high signal density leads to cell recruitment, manifested by G1 and S phase shortening and, ultimately, reduction of cell cycle length. In contrast to our previous article, we now assume that the recruitment sensitivity S_R is finite (defined as the inverse of the minimal signal density required to recruit an ependymal cell, ρ_s^{min}, Fig. 1 C). We arbitrarily considered that cells are not exposed to the signal if there are less than two signalling particles around them. We supposed that cell recruitment is irreversible and inherited by the daughter cells. Thus, in our model, spinal cord growth during regeneration is driven by ependymal cell proliferation, in turn controlled by the signal diffusing from the spinal cord regenerating tip towards the anterior side while irreversibly recruiting new ependymal cells. We first validated the cellular scale of the model by by comparing our model results with the model of [17] (Supplementary section 3, Fig. S1 A, B). Next, we validated the numerical scheme of the reaction-diffusion process governing the signaling scale of our model by comparing the 1D density profile of the signal with the analytical solution of the reaction-diffusion model in a finite domain (without ependymal cell proliferation), derived following our method previously reported [17] (Supplementary section 4, Fig. S2). After both scales of the model were validated, we evaluated whether the full model could generate a dynamical behavior consistent with the regenerative response observed in the axolotl spinal cord after amputation. Our simulations showed that the spatial distribution of the signal is shifted posteriorly as the spinal cord expands, result qualitatively equivalent to that previously reported [7] (Fig. 2 A, B, Supplementary Movie 1).

2.2 Axolotl spinal cord regeneration can be quantitatively explained by a signal operating under a reaction-diffusion regime

By exploring the model parameters space we observed that the evolution of spinal cord outgrowth is controlled by the interplay between the diffusion coefficient D and the degradation constant k

(Fig. 2 C, C' and C", Supplementary Movie 2). Indeed, decreasing the degradation constant (for a fixed diffusion coefficient value) is followed by an increase of the tissue outgrowth (compare Fig. 2 C and C'). On the contrary, decreasing the diffusion speed (while fixing the degradation) led to a remarkable decrease of the tissue outgrowth (compare Fig. 2 C' and C"). Thus, there is an optimal balance between the diffusion of the signal (that governs the speed of the signal spreading and therefore the recruitment of new cells) and its degradation constant (that prevents the signal to travel too far during its half-life) that shapes the simulated regenerative response.

To gain a quantitative understanding of the regenerative response of the axolotl spinal cord, we fully parametrized the model. To that aim, we fixed the model parameters controlling the cell cycle paces and cellular geometry by using our previously reported experimental data obtained from ependymal cells in regenerating and uninjured spinal cords [5] (see Table S1). Since the signal here proposed is hypothetical, we considered D, k and S_R as free parameters and explored the resulting model parameters space.

To assess if the model could explain the regenerative response of the axolotl spinal cord and to simultaneously estimate the free parameters, we fitted the model to the previously reported experimental recruitment limit, defined as the spatial position (in the AP axis) separating the (posterior) high-proliferation region from the (anterior) low-proliferation region [6] (for details of the fitting procedure, see Supplementary section 7). To this aim, we tracked the AP-axis position of the most anteriorly recruited cell in our simulations, denoted as $\xi(t)$, and referred to it as the theoretical recruitment limit (following [7]). The model-predicted recruitment limit successfully reproduced the experimental switchpoint with best-fitting parameters $D = 1\ \mu m^2/s$, $\rho_s^{min} = 3$ and $k = 1$ days^{-1} (where the half-life is 0.7 days) (Fig. 2 D). Importantly, this parametrization leading to the best-fitting of the switchpoint curve quantitatively predicted the time course of tissue outgrowth observed *in vivo* [6] (Fig. 2 E). We found that there is a zone within the parameter space that allows the experimental switchpoint curve to be recovered (Fig. 2 F). This zone remarkably recapitulates the experimental outgrowth at day 6 (Fig. 2 G). Indeed, the distance between the experimental and the simulated recruitment limit curves (denoted by $E(\boldsymbol{\xi}, \boldsymbol{C_e})$ and defined in Eq. (S.20) in Supplementary section 7) is minimal in a region along the curve $\sqrt{D/k} = 270\ \mu$m corresponding to the best-fitting parameter values (Fig. 2 F). In this zone of the parameters space, we find the best agreement between the experimental spinal cord outgrowth at day 6 and the simulated outgrowth predicted by our model (Fig. 2 G). Altogether, these results suggest that spinal cord regeneration could be mainly controlled by a signal created at the (moving) boundary of the tissue while evolving via a reaction-diffusion process and recruiting cells as it spreads over the spinal cord. New cells are locally activated by the presence of this signal, accelerating tissue growth. In this scenario, the speed of tissue expansion is mainly controlled by the interplay between diffusion and degradation of the signal via the quantity $\sqrt{D/k}$. This quantity is well known in developmental biology in the cases of exponential morphogen gradient formation and referred to as the Characteristic Length λ [14]. It corresponds to the distance between the signal source (in our case, the posterior border of the tissue) and the position at which a concentration profile exponentially decaying equals a fraction $1/e$ of its concentration at the source.

2.3 The regenerative response of the spinal cord can be modulated by the cell sensitivity to the signal

In the previous section, we assumed a relatively small value of ρ_s^{min} which results on extreme sensitivity of the ependymal cells to the signal density. Higher values of this parameter reduce

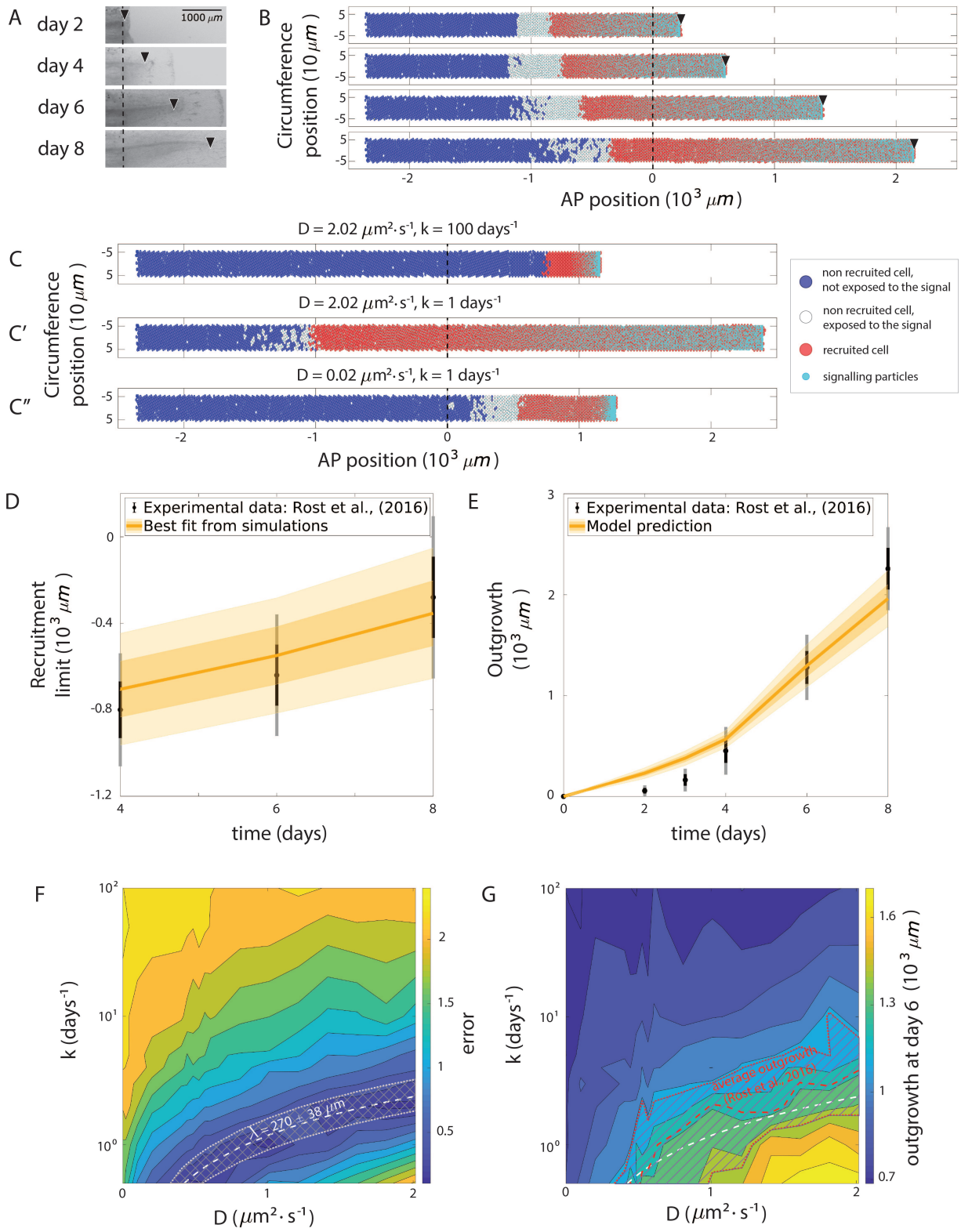
A
day 2
day 4
day 6
day 8
1000 μm
B
Circumference position (10 μm)
AP position (10³ μm)
C
C′
C″
D = 2.02 μm²·s⁻¹, k = 100 days⁻¹
D = 2.02 μm²·s⁻¹, k = 1 days⁻¹
D = 0.02 μm²·s⁻¹, k = 1 days⁻¹
non recruited cell, not exposed to the signal
non recruited cell, exposed to the signal
recruited cell
signalling particles
D
Experimental data: Rost et al., (2016)
Best fit from simulations
Recruitment limit (10³ μm)
time (days)
E
Experimental data: Rost et al., (2016)
Model prediction
Outgrowth (10³ μm)
time (days)
F
k (days⁻¹)
D (μm²·s⁻¹)
error
λ = 270 ± 38 μm
G
k (days⁻¹)
D (μm²·s⁻¹)
outgrowth at day 6 (10³ μm)
average outgrowth (Rost et al., 2016)

Figure 2:

Figure 2. **Axolotl spinal cord regeneration can be qualitatively and quantitatively explained by a signal operating under a reaction-diffusion regime.** **(A)** Images of a regenerating spinal cord upon tail amputation at different times post amputation(modified from [6], Figure 1A). Scale bar, 1000 μm. **(B)** Simulations of the modelled regenerating spinal cord after tail amputation at the indicated times. In (A, B), the black dashed line represents the amputation plane while the black arrowheads indicate the tip of the regenerating spinal cord. Ependymal cells are represented as discs and colored using a French flag-like code, as explained in the legend of Figure 1. B,C. Smaller cyan discs represent the signalling particles. Signal diffusion coefficient $D = 1\ \mu m^2 \cdot s^{-1}$, degradation rate $k = 1$ days^{-1} and $\rho_s^{min} = 3$. **(C,C',C")** Simulation results at day 8 post amputation: large diffusion and degradation of the signal (C), large diffusion and small degradation of the signal (C'), small diffusion and degradation of the signal (C"). Same representation as in panel (B). **(D)** Model-predicted time course of recruitment limit (yellow) fitted to the experimental counterpart [6] (black). **(E)** Model-predicted time evolution of the spinal cord outgrowth (yellow) and the experimental counterpart [6] (black). (D) and (E): for the model predictions, means are represented as solid lines and each shaded area corresponds to 1 standard deviation out of the best fitting simulations identified following the procedure described in Supplementary Section 7); for the experimental data, means are represented by points while error bars represent the standard deviation of the recruitment limit posterior distribution in (D) and the standard deviation of the outgrowth measurements in (E), both obtained from the experiments reported in [6]. Black error bars correspond to 1 σ while grey error bars correspond to 2σ. **(F)** Phase portrait depicting the error between the model-predicted recruitment limit and the experimentally measured one [6] at day 6, as a function of the diffusion coefficient D (x-axis) and the degradation rate k (y-axis), with the curve $\sqrt{D/k} = 270 \pm 38\ \mu m$ superimposed. **(G)** Phase portrait showing the tissue outgrowth predicted by the model at day 6 post amputation as a function of the diffusion coefficient D (x-axis) and the degradation rate k (y-axis), with the experimental outgrowth from [6] (mean is represented by the red dashed line, the striped area corresponds to 1 standard deviation, obtained from the experiments as reported in [6]) and the curve $\sqrt{D/k} = 270\ \mu m$ (white dashed line) superimposed.

the cell sensitivity to the signal (Supp. Fig. 3 A). In this section we investigated the role of the cell to signal sensitivity on the emergent regenerative outgrowth, by exploring the values of the parameter ρ_s^{min} in the range indicated in Table S1. As expected, decreasing the sensitivity of cells to the signal leads to a reduction in the recruitment limit that reduces the spinal cord outgrowth (Fig. 3 A, A', Supplementary Movie 3). The pool of recruited cells that activate their high proliferation program is directly linked to the ability of individual cells to measure the signal density around them. This result shows that the main component of tissue regeneration lies in the pool of recruited ependymal cells, the size of which is controlled by the signal properties and the cells sensitivity to the signal.

We set out to determine quantitatively the influence of the ependymal cells sensitivity to the signal on spinal cord regeneration in the axolotl. To achieve this, we observed the outgrowth predicted by the model at day 6 post amputation, within the surface of the parameters space corresponding to the diffusion coefficient and the cell-to-signal sensitivity (Fig. 3 B and Supp. Fig. 3 B). We observed that decreasing the cell-to-signal sensitivity (by increasing ρ_s^{min}) from the best-fitting value (that coincides with the experimental response previously observed at that time ([6])) leads to the reduction of the outgrowth predicted at day 6 (Fig. 3 B and C). Interestingly, the model predicts that reducing the cell-to-signal sensitivity in 92.5% leads to a spinal cord outgrowth in agreement with that measured in the axolotl when the neural stem cell marker Sox2 is knocked-out ([18]) (Fig. 3 B, C). Thus, our computational model of the axolotl spinal cord governed by cell cycle acceleration, in turn controlled by a reaction-diffusion signal, was validated by fitting to the previously reported experimental recruitment limit curve and correctly predicted spinal cord outgrowth observed under regenerative conditions. Importantly, our model gives a conceptual framework to interpret the lack of regenerative response of the Sox2 knock-out axolotls by turning down the sensitivity of the ependymal cells to the signal.

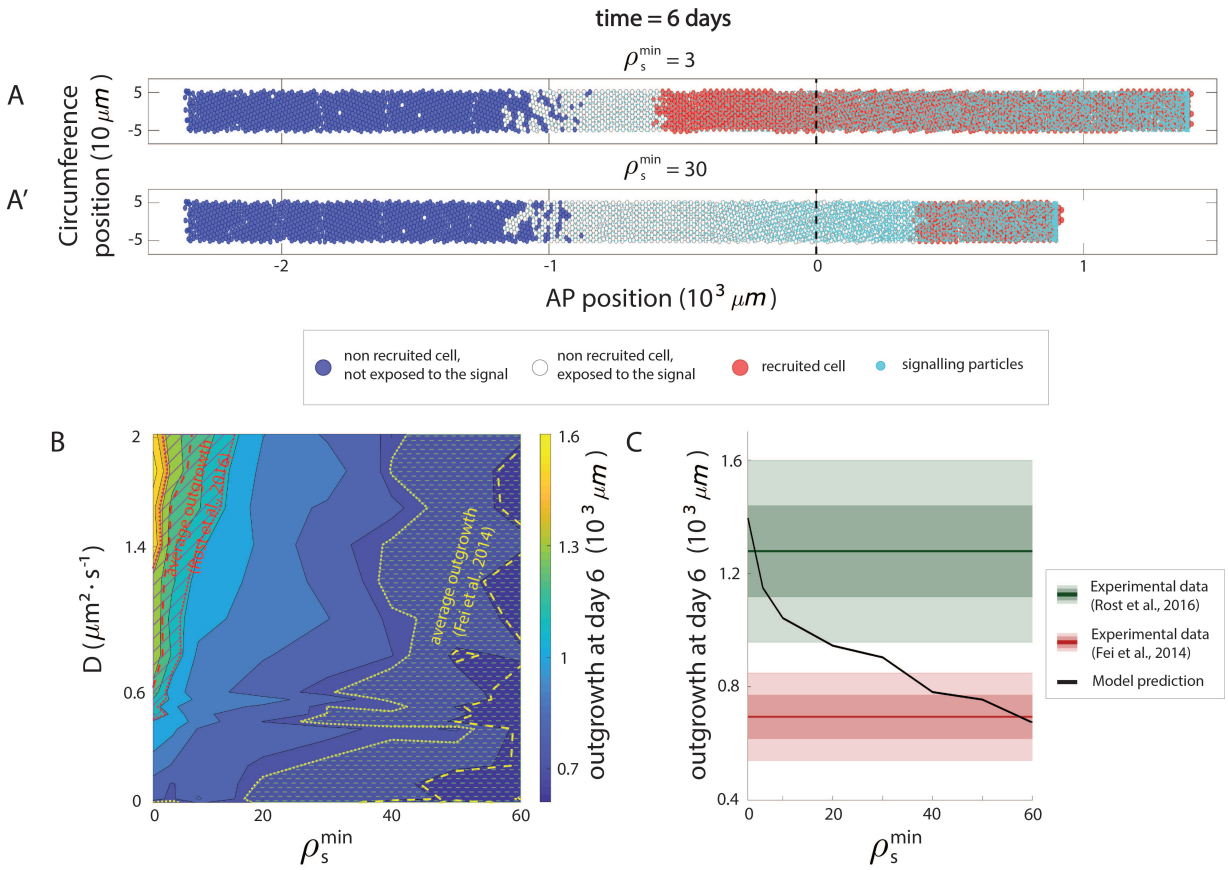

Figure 3: **The regenerative response of the spinal cord can be modulated by the cell sensitivity to the signal. (A, A')** High cell-to-signal sensitivity (small $\rho_s^{min} = 3$, A) results in a higher recruitment limit (the domain of red recruited cells and outgrowth) compared to low cell-to-signal sensitivity (large $\rho_s^{min} = 30$, B). In (A, A'), model simulation results of the regenerating spinal cord at day 6 post amputation. Ependymal cells are represented as discs and colored using a French flag-like code, as explained in the legend of Figure 1 B,C. **(B)** Phase portrait showing the model-predicted spinal cord outgrowth at day 6 for $k = 1$ days^{-1} as a function of the cell-to-signal sensitivity ρ_s^{min} (x-axis) and the signal diffusion coefficient D (y-axis), with experimental measurements of [6] (red) and [18] (yellow) superimposed. **(C)** Spinal cord outgrowth at day 6 post amputation as a function of the cell-to-signal sensitivity ρ_s^{min}. Decreasing the cell-to-signal sensitivity reduces the spinal cord outgrowth predicted at time 6 post amputation from values consistent with normal regenerative conditions [6] (green) to those corresponding to impeded regeneration by knocking out SOX2 [18] (red). Means are represented as lines and each shadowed area corresponds to 1 standard deviation. In (A, C), signal diffusion coefficient $D = 1$ $\mu m^2 \cdot s^{-1}$ and degradation rate $k = 1$ days^{-1}.

2.4 The control of spinal cord regeneration lies in the characteristic length of the signal and the cell-to-signal sensitivity.

The previous sections showed that spinal cord regeneration in the axolotl can be quantitatively explained in terms of cell cycle acceleration of ependymal cells, controlled by a signal operating under a reaction-diffusion mechanism. This could imply that the control of the regenerative response relies on the three model parameters, the diffusion coefficient, the degradation constant/half-life of the signal and the cell-to-signal sensitivity. Nevertheless, visual inspection of Fig. 2 F, G depicts a clear domain identified by the characteristic length λ that recapitulates both the experimental switchpoint and the outgrowth at day 6. This suggests that the regenerative response is not controlled by the diffusion coefficient, half-life of the signal and cell-to-signal sensitivity, but rather by this sensitivity and λ. To test this hypothesis, we used our computational model to predict the regenerative response at a fixed time (We have arbitrarily chosen day 8) for different combinations of signal-related parameters and plotted the spinal cord outgrowth as a function of the characteristic length (Fig. 4 A). Interestingly, our results showed that the tissue outgrowth is almost an affine function of λ (*i.e.*, showing a linear correlation with λ), the slope of which depends on the cell-to-signal sensitivity. This result indicates that the control of the regenerative response falls on the signal characteristic length and the sensitivity of the cells to the signal.

The cell-based computational model developed in previous sections assumes that the signal recruits cycling cells by reducing G1 and S phase, which accelerates their cell cycle, expanding the spinal cord tissue where the signal operates, as previously reported [7]. Thus, we wondered whether the control of the regenerative response by the characteristic length of the signal and cell-to-signal sensitivity could be an intrinsic feature of the non-Markovian cell cycle dynamics of the cell-based computational model. To explore this hypothesis, we simplified our cell-based computational model by approximating the more correct cell division mechanism with a random (Poisson) process of signal-dependent frequency (see Supplementary Section 5 for more details). Importantly, we observed that the seemingly linear correlation between the regenerative outgrowth and the signal characteristic length is preserved (Fig. 4 B). Although the Poisson-based model is definitely less biologically relevant to describe the regenerative response in the axolotl spinal cord, its simplicity makes it ideal to theoretically understand the linear dependence of the tissue outgrowth with the signal characteristic length, where the slope depends on the cell-to-signal sensitivity. In this vein, we developed a theoretical framework of the regenerative growth controlled by a signal whose dynamics is under a reaction-diffusion mechanism.

We formally considered the case of instantaneous signal diffusion and degradation (ideally infinite values of D and k, corresponding to an instantaneous relaxation of the signal profile towards its steady state). We obtained analytical expressions for the tissue domain occupied by the recruited fast proliferating cells L_f and the domain occupied by non-recruited slow proliferating cells L_s as functions of time (see formal derivation in Supplementary section 6):

$$L_f(t) = -\xi(0)e^{\nu_F t}, \tag{2}$$

$$L_s(t) = (\xi(0) + L_0)e^{\nu_S t}. \tag{3}$$

In these expressions, L_0 is the initial length of the spinal cord tissue, immediately after amputation (defined as the distance between the most anterior boundary of the domain and the amputation plane) whereas $\xi(0) < 0$ is the position of the recruitment limit at time zero; (*i.e.*, the spatial point in the AP axis separating the populations of non-recruited and recruited cells

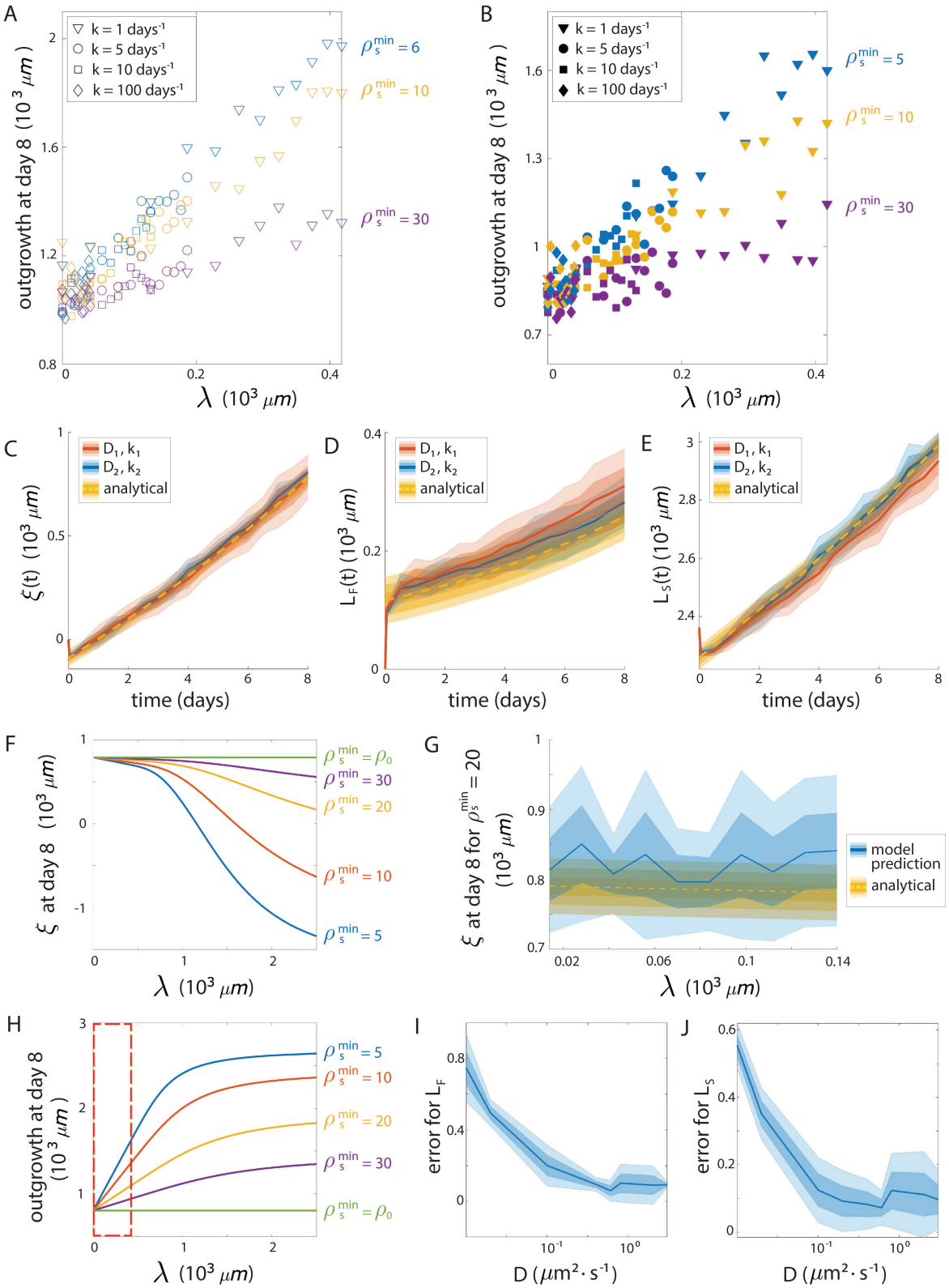
A
k = 1 days-1
k = 5 days-1
k = 10 days-1
k = 100 days-1
outgrowth at day 8 (10^3 μm)
λ (10^3 μm)
B
C
D
E
D1, k1
D2, k2
analytical
ξ(t) (10^3 μm)
L_F(t) (10^3 μm)
L_S(t) (10^3 μm)
time (days)
F
ξ at day 8 (10^3 μm)
G
ξ at day 8 for ρ_s^min = 20 (10^3 μm)
model prediction
H
I
J
error for L_F
error for L_S
D (μm²·s⁻¹)

Figure 4:

Figure 4: **The control of spinal cord regeneration lies in the characteristic length of the signal and the cell-to-signal sensitivity. (A)** Spinal cord outgrowth predicted by the computational model as function of the characteristic length λ of the signal for different values of the signal degradation rate k ($k = 1$ day^{-1} (triangle markers), $k = 5$ day^{-1} (round markers), $k = 10$ day^{-1}(square markers), $k = 100$ day^{-1} (diamond markers). **(B)** Tissue outgrowth of the computational model assuming Poisson-based cell divisions, same legend as for panel (A). **(C,D,E)** Recruitment limit of the Poisson-based model as a function of time for two sets of parameters (D, k) with the same $\lambda = 41.74$ μm (orange and blue) compared with the corresponding analytical solution (yellow dashed line and shadowed areas, each shadowed area corresponds to one ependymal cell diameter) (C). Same representation for the length of the fast-cycling population $L_F(t)$ (D) and the slow-cycling population $L_S(t)$ (E). In (C), (D) and (E), for each set of parameters (D, k), means are represented as lines and each shadowed area corresponds to 1 standard deviation out of 5 simulations. **(F,H)** Theoretical predictions of the recruitment limit $\xi(t)$ (F) and tissue outgrowth (H) as a function of λ, for different values of the cell-to-signal sensitivity (ρ_s^{min}). **(G)** Theoretical prediction (yellow) of the recruitment limit $\xi(t)$ at time $t = 8$ days post amputation as a function of λ superimposed with the simulated values using the Poisson-based computational model (blue), for $\rho_s^{min} = 20$ (mean is represented as solid line and each shadowed area corresponds to 1 standard deviation out of 10 simulations). **(I,J)** Error between the theoretical and the numerical values obtained with the Poisson-based computational model of the fast-cycling population length $L_F(t)$ (I) and slow-cycling population length $L_S(t)$ (J) at time $t = 8$ days as function of the diffusion coefficient D for fixed value of $\lambda = 41.74$ μm. In (I) and (J) means are represented as lines and each shadowed area corresponds to 1 standard deviation out of 5 simulations.

(Note that we are using a coordinates system centered in the amputation plane, see Supp. Fig. 4). We found that $\xi(0)$ is defined by:

$$\xi(0) = \lambda \ \sinh^{-1}\left(\frac{\rho_s^{min}}{\rho_0}\sinh\left(\frac{L_0}{\lambda}\right)\right) - L_0 \tag{4}$$

Since the signal lives on the domain occupied by the ependymal cells, we require that $\lambda < L_0$. By using Eqs. (2)-(4), we can directly write the theoretical spinal cord outgrowth as a function of time as

$$\text{Outgrowth}(t) = L_s(t) + L_f(t) - L_0. \tag{5}$$

To evaluate the merits of our theory, we decided to test it by comparing the theoretical predictions with simulations of the Poisson-based computational model for large enough values of D and k. Remarkably, we obtained a very good correspondence between the theoretical values of $\xi(t)$ (see the general expression of Eq. (4) in Supplementary section 6), $L_s(t)$ and $L_f(t)$ and their corresponding values computed on the simulations, for all times t (Fig. 4 C-E).

This novel theory of spinal cord regeneration allows us to demonstrate how cell recruitment depends on the signal characteristic length as well as the cell to signal sensitivity at a given time (Fig. 4 F). First, by classical asymptotic arguments, one directly obtains that the recruitment limit $\xi(0)$ gets closer to 0 immediately after amputation, as the signal characteristic length tends to zero. These results are expected since without diffusion, $D = 0$, the signal is only present on the posterior boundary of the spinal cord and only a small fraction of the population accelerate its cell cycle. Moreover, Eq. (4) reveals how the cell sensitivity to the signal controls the regenerative response. First, notice that $\rho_s^{min} = \rho_s^0$ (the density of the signal at the front) leads to $\xi(0) = 0$ (Fig. 4 F). Again, in this case, the cells can only be recruited if the signal density is larger than the one prescribed on the front, i.e., only the cells at the very spinal cord front will accelerate their cell cycles and this leads to the same behavior as a non-diffusive signal ($D = 0$). As ρ_s^{min} increases, so does $\xi(0)$, indicating that higher sensitivity of tissue cells to the signal leads to larger outgrowth (Fig. 4 F). Finally, plotting the theoretical value of the outgrowth given by (5)-(4) as function of λ (Fig. 4.H) showed that indeed for small values of λ (red box corresponding to the range of λ used for our simulations), the outgrowth evolved almost linearly with λ, the slope depending on the threshold density ρ_s^{min}.

We further validated the formal derivation by comparing the theoretical dependence of the recruitment limit $\xi(t)$ on the signal characteristic length with that dependence observed from simulations using the Poisson-based computational model (Fig. 4 G). We obtained a very good agreement between the theory and the simulations for different values of cell to signal sensitivity (Fig. 4 G). It is noteworthy that we were only able to perform simulations for $\lambda < 400$ μm because of computational time limitations. Indeed, as the characteristic length increases, the numerical time-step required for the simulation decreases, leading to an increase of the overall computation time.

By using our new theory (Eqs. (2) - (5)), we represented the predicted spinal cord outgrowth at a given time (8 days post amputation) as a function of the signal characteristic length, for different cell to signal sensitivities. Remarkably, our results demonstrate that both magnitudes are linearly correlated for characteristic lengths approximately smaller than 400 μm (see the rectangle within Fig. 4 H), with a slope depending on the cell sensitivity to the signal ρ_s^{min}, in good agreement with our simulation results (Fig. 4 A, B). However as our theory predicts, the tissue length evolves as a saturated exponential for larger values of λ. This saturation effect is due to the finite size of the initial domain for ependymal cells. As the signal invades the domain, it recruit more cells up until reaching the anterior boundary where no more cells can be recruited anymore, saturating the overall evolution of the tissue.

Finally, to investigate the limitations of our theory, we determined the regime within the parameters space in which the theoretical derivation is valid. As the theoretical derivation was made under the regime of instantaneous reaction-diffusion of the signal (*i.e.*, high diffusion coefficient and degradation rate), we expected that the numerical simulations get closer to the theoretical predictions as the time scale of the reaction-diffusion process dominates the time scale of cell division. To this aim, we arbitrarily fixed the value of the signal characteristic length $\lambda = 41.74\mu$m and computed the error, as defined in Eq. (S.20) in Supplementary Section 7, between the theoretical and simulated tissue domains occupied by the recruited fast proliferating cells L_f and the domain occupied by non-recruited slow proliferating cells L_s, for different values of the diffusion coefficient D. As expected, we observed that the error decreases as the diffusion coefficient increases (Fig. 4 I, J).

Taken together, the results of this section explain why the regenerative spinal cord outgrowth is approximately linear with the signal characteristic length for a given cell to signal sensitivity. Our theoretical results demonstrate that the regenerative response of the modelled spinal cord is determined by the sensitivity of the cells to the signal, and is not controlled by the diffusion coefficient of the signal and its half-life, but rather by the characteristic length of the signal.

3 Discussion

Severe trauma of the spine leads to irreversible and usually irreparable consequences in most vertebrates. In humans, these traumatic injuries often have dramatic repercussions not only for the patients suffering from those injures but also for their families who take on caring responsibilities for the patients. These overwhelming consequences observed in humans after traumatic injuries in the spine strikingly contrast with the complete structural and functional regeneration of the spinal cord displayed by the axolotl after the most extreme possible injury: tail amputation. Why this salamander is capable of such remarkable regeneration traits while we are not is still elusive [19].

By combining a very simple 1D computational model with functional experiments using FUCCI

technology in axolotls, we previously showed that regeneration of the spinal cord in the axolotl is consistent with a process of ependymal cell recruitment triggered by a so far unknown signal that propagates $\approx 830\mu$m anteriorly from the injury site during ≈ 85 hours post amputation [7]. However, the signal and the precise mechanism of its propagation within the axolotl spinal cord have not yet been elucidated.

During development, numerous tissues are shaped through morphogenetic processes controlled by morphogens or signals whose dynamics are governed by reaction-diffusion processes. As an example, growth regulation of the Drosophila wing imaginal disc is governed by the Decapentaplegic (Dpp) morphogen gradient, in turn ruled by a reaction-diffusion mechanism [20]. In vertebrates, a reaction-diffusion system explains the dynamics of the transforming growth factor–β superfamily signals Nodal and Lefty during zebrafish embryogenesis [21]. In a chick embryo, a reaction-diffusion mechanism was proposed to explain the antagonistic effect of BMP2 and BMP7 on the feather patterning [22]. These and other examples show that the reaction–diffusion models constitute effective and accurate mathematical constructs guiding mathematical approaches in development [23] and possibly in regeneration [12]. Thus, it is conceivable that the particular spatiotemporal distribution of the signal responsible for the regenerative response observed in the axolotl spinal cord might reflect a reaction-diffusion mechanism at work. This is why, in this theoretical study, we decided to test this hypothesis.

To that aim, we have developed a 2D multi-scale hybrid computational model featuring ependymal cells which interact with a signal continuously produced at the posterior tip of the spinal cord, which diffuses within the tissue while being consumed with a given degradation rate. When the local signal density overcomes a certain threshold, the ependymal cells in contact with the signal accelerate their cell cycle, increasing the overall tissue growth speed (Fig. 1). After validating both the cellular and the signalling scales individually (Supplementary sections 3 and 4), we tested the model by fitting the previously reported recruitment limit curve [6]. Interestingly, the model is able to recover the spinal cord outgrowth experimentally observed [6] (Fig. 2 F, G, Fig. 3 B, C, Supp. Fig. 3 B), and allowed us to have a first estimate of the biophysical parameters governing the hypothetical signal responsible for the regenerative process observed in the axolotl spinal cord. The predicted signal diffusion coefficient and half-life are $\approx 1\mu\text{m}^2\text{sec}^{-1}$ and $\approx 1,000$ min, respectively. While there are no measurements of diffusivity or stability of morphogenetic signals in the axolotl during regeneration, these biophysical parameters were determined for a variety of morphogens in zebrafish embryos *in vivo*. As an example, the diffusion coefficients of Cyclops, Squint, Lefty1 and Lefty2 were estimated in ($\mu\text{m}^2\text{sec}^{-1}$) 0.7 ± 0.2, 3.2 ± 0.5, 11.1 ± 0.6, and 18.9 ± 3.0, respectively, while their half-lives ranged from (min) 95 to 218 in the blastula stage during zebrafish embryogenesis [21]. Interestingly, in the same animal model, BMP2b and Chordin have clearance rate constants of ($10^{-5}s^{-1}$) 8.9 ± 0.1 and 9.6 ± 0.3, corresponding to half-lives of (min) 130 and 120, and effective diffusion coefficients of ($\mu\text{m}^2\text{sec}^{-1}$) 2–3 and 6–7, respectively [24]. Hence, the diffusion coefficient and half-life of the hypothetical signal predicted by our model are within the same order of magnitude than Cyclops and BMP gradients determined in the zebrafish embryo. In particular, our results show that the hypothetical signal governing spinal cord regeneration has half the diffusion coefficient of BMP observed during zebrafish embryogenesis and about seven times its half-life. These differences could be attributed to the differences in animals, stage and anatomical orientation (anterior-posterior axis in the axolotl spinal cord versus dorsal-ventral axis in the zebrafish embryo) or they could of course reflect different signals.

Importantly, our computational model results indicate that the regenerative growth response

scales with the characteristic length of the signal, where the slope depends on the ependymal cell-to-signal sensitivity (Fig. 4 A), result that was also recapitulated when the proliferative response of the ependymal cells was simulated with a naïve Poisson-based proliferation model (Fig. 4 B). To explain this result, we developed a theory that allowed us to unveil a profound feature of the regenerative response displayed by the computational model. Our rigorous mathematical demonstration reveals that the spinal cord outgrowth emerging during regeneration in the axolotl can be controlled by the characteristic length of the signal rather than by its individual diffusion coefficient or half-life. This study predicts that the signal governing the regenerating spinal cord in the axolotl has a characteristic length of about 270 μm. Interestingly, gradients of BMP and Chordin display characteristic lengths of 168 and 260 μm, respectively (calculated from [24]), suggesting that the our regeneration-inducing signals could operate within the BMP pathway.

Noteworthy, the reaction-diffusion mechanism under consideration here may be an effective mechanism arising from a process which does not necessarily involve morphogen gradients. Indeed, there is a growing appreciation that morphogenetic processes can be moulded by physical cues [25]. A clear example is the fluid-to-solid jamming transition observed during posterior axis elongation in zebrafish embryos [26]. In this system, there is a transition of rigidity from anterior to posterior tissues where the fluid-like posterior tissues remodel before their maturation. A similar process takes place during development of the zebrafish blastoderm where the rigidity transitions from a network of high to low intercellular adhesions [27]. Hence, the reaction-diffusion mechanism governing our hypothetical signal responsible for spinal cord regeneration after amputation could correspond to a mechanical process. Interestingly, a mechanical reaction-diffusion mechanism elegantly explains wound-induced regeneration of hair follicles in mice [28]. In fact, the idea was already anticipated in the seminal study of George Oster, James D. Murray and Albert K. Harris [29] that showed pattern formation emerging from cell motility and rigidity perturbations, very much like reaction-diffusion instabilities predicted by the Gierer-Meinhardt [30] and the Turing models [31].

3.1 Limitations of this study, future perspectives and conclusion

The computational 2D cell-based computational model here developed focused on the early regenerative response of the spinal cord in the axolotl. A control mechanism via a negative feedback process effectively turning down proliferation, and thus regeneration must exist within the subsequent weeks post amputation. Indeed, in the second week of regeneration, asymmetric cell divisions of the ependymal cells are observed [5]. Hence, to address the regenerative response of the spinal cord in the long-term, the radial direction of the ependymal tube needs to be considered and a 3D model will become thus inevitable. A possible strategy to circumvent the resulting complexity of the spinal cord during this later regulatory phase of regeneration could involve mapping the cell-based computational models with a macroscopic (continuous) description, as those used in [32, 33, 34]. Additionally, the theory demonstrating that the regenerative growth scales with the characteristic length of the signal relies on the fast diffusion and reaction approximation. Future studies should address whether this scaling extends to other reaction-diffusion regimes. This study shows that spinal cord regeneration in the axolotl can be orchestrated by a hypothetical signal operating under a reaction-diffusion scheme under the control of its characteristic length and the sensitivity of the ependymal cells to the signal. Further investigation is required to unveil the nature of the signal to then explore how conserved and thus general this mechanism of regeneration might be.

4 Author contributions

5 Acknowledgements

V.C. was supported by Institut national de recherche en informatique et en automatique (Inria) Paris. D.P. was supported by Sorbonne Alliance University with an Emergence project MATHREGEN, grant no. S29-05Z101 and by Agence Nationale de la Recherche (ANR) under the project grant number ANR-22-CE45-0024-01. OC was funded by grants PICT-2017-2307 and PICT-2019-03828) from the Agencia Nacional de Promoción Científica y Tecnológica of Argentina. The authors sincerely thank Alberto Ceccarelli, Leo Otsuki, Sophie Hecht and Fabian Rost for their careful reading of the manuscript and their excellent suggestions, as well as Elly Tanaka for incessant and stimulating discussions.

6 Declaration of interest

7 Computational methods

7.1 Multi-scale hybrid computational model of spinal cord regeneration in the axolotl

Details on the modelling aspects and numerical methods used concerning the 2D computational model are given in Supplementary section 2.

7.2 Validation of the cellular scale of the computational model

Details on the validation of the cellular scale of the model in 1D, through the comparison by previously reported results [7] are provided in Supplementary section 3.

7.3 Validation of the signalling scale of the computational model

Details on the validation of the numerical scheme for the reaction-diffusion process of the signal through the comparison of our 1D signal density profile with the analytical solution of the reaction-diffusion model in a finite domain [17] can be found in Supplementary section 4.

7.4 Model variant with a Poisson-based cell division process

Details on the modelling aspects and numerical methods used concerning the variant of the mathematical model where ependymal cell divisions follow a Poisson process are given in Supplementary section 5.

7.5 Theoretical prediction of the spinal cord outgrowth driven by an instantaneous reaction-diffusion signal

Details on the theoretical framework developed to account for the spinal cord outgrowth controlled by a signal operating in an instantaneous reaction-diffusion regime are reported in Supplementary section 6.

7.6 Model fitting to the experimental recruitment limit curve

Details on the procedure used to fit the model to the previously reported experimental switch-point [6] are given in Supplementary section 7.

7.7 Error between simulated and analytical curve

Details on the definition of the error between a simulated and an analytical curve are given in Supplementary section 8.

8 Legends of Supplementary Figures and Movies

Figure S2: Related to Figure 2 and Section 2.1 of the main text. **(A,B)** Scheme showcasing two cases where ependymal cell i (cyan disc) is a front cell (panel A) or not (panel B), using the identification rule described in section S2.1. **(C)** Comparison between the outgrowth predicted by our simplified 1D model (red shadowed area) and by [7] (cyan error bar). Each prediction has been obtained averaging over 100 replicates. Means are represented as lines, shadowed area and error bar correspond to 1 standard deviation. **(D,E,F)** Comparison between the 1D density profile of signalling particles (both the mean - blue solid line - and the standard deviation - blue shaded area - are calculated from the y-axis at each x position) with the analytical solution $C_1(z,t)$ (Eq. (S.16), which can be found in Supplementary section 4) of the reaction-diffusion model in finite domain (orange solid line). For $D = 0.6\ \mu m^2 \cdot s^{-1}$, $k = 1$ days^{-1}, at different times (from top to bottom: day 0.02, day 0.2, day 4).

Figure S3: Related to Figure 3 and Section 2.3 of the main text. **(A)** Cell activation function as function of the local sensitivity of the ependymal cells, for different sensitivity levels to the signal (parameter ρ_s^{min}). The maximal signal density (imposed on the right boundary, i.e. on the spinal cord front) is indicated in red. For small sensitivity to the signal (large ρ_s^{min}, yellow curve), no cells will be recruited by the signal, while for large sensitivity (small ρ_s^{min}, blue curve), the majority of cells exposed to the signal will be recruited instantaneously. **(B)** Error between the model predicted recruitment limit and experimental recruitment limit curve [5] as function of the sensitivity to the signal ρ_s^{min} (x-axis) and the diffusion coefficient D (y-axis).

Figure S4: Related to Figure 4 and Section 2.4 of the main text. Tissue domain occupied by recruited fast proliferating cells ($L_F(0)$), tissue domain occupied by non-recruited slow proliferating cells ($L_S(0)$) and recruitment limit ($\xi(0)$) at time 0. The x-axis represents the AP axis, the blue curve is the density of the signal. The amputation plane is indicated by a dashed black line. The signal sensing threshold (ρ_s^{min}) for cell recruitment is indicated in cyan.

Supplementary Movie 1: Simulation of the modelled regenerating spinal cord after tail amputation. Related to Figure 2 and Section 2. Signal diffusion coefficient $D = 1$ $\mu m^2 \cdot s^{-1}$, degradation rate $k = 1$ days^{-1} and $\rho_s^{min} = 3$. Ependymal cells are represented as discs depicted in three colors: blue, if they are non recruited (slow-cycling) and not exposed to the signal; white, if they are non recruited (slow-cycling) even if exposed to the signal; red, if they are recruited (fast cycling cells). Smaller cyan discs represent the signalling particles. The black dashed line represents the amputation plane.

Supplementary Movie 2: The evolution of spinal cord outgrowth is controlled by the interplay between the diffusion coefficient D and the degradation constant k. Related to Figure 2 and Section 2. Simulations of the modelled regenerating spinal cord after tail amputation: large diffusion ($D = 2.02\ \mu m^2 \cdot s^{-1}$) and large degradation ($k = 100$ days^{-1}) of the signal (top), large diffusion ($D = 2.02\ \mu m^2 \cdot s^{-1}$) and small degradation ($k = 1$ days^{-1}) of the signal (middle), small diffusion ($D = 0.02\ \mu m^2 \cdot s^{-1}$) and small degradation ($k = 1$ days^{-1}) of the signal (bottom). The cell-to-signal sensitivity is fixed in $\rho_s^{min} = 3$. The black dashed line represents the amputation plane. Ependymal cells are represented as discs depicted in three colors: blue, if they are non recruited (slow-cycling) and not exposed to the signal; white, if they are non recruited (slow-cycling) even if exposed to the signal; red, if they are recruited (fast cycling cells). Smaller cyan discs represent the signalling particles.

Supplementary Movie 3: Tissue regeneration can be modulated by the cell sensitivity to the signal. Related to Figure 3 and Section 2. Simulations of the regenerating spinal cord after tail amputation. Signal diffusion coefficient $D = 1\ \mu m^2 \cdot s^{-1}$ and degradation rate $k = 1$ days^{-1}. Ependymal cells are represented as discs depicted in three colors: blue, if they are non recruited (slow-cycling) and not exposed to the signal; white, if they are non recruited (slow-cycling) even if exposed to the signal; red, if they are recruited (fast cycling cells). Smaller cyan discs represent the signalling particles. At the top, for large sensitivity to the signal (small $\rho_s^{min} = 3$), a large zone of high proliferative cells is observed. At the bottom, for small sensitivity to the signal (large $\rho_s^{min} = 30$), only cells close to the front are activated.

9 Data and code availability

The computational model in this study was implemented in Fortran 90 while visualization of simulations and analyses were executed with MATLAB. Source codes for simulations and post-processing can be found at: https://doi.org/10.5281/zenodo.8111099.

References

[1] L. Spallanzani, Prodromo di un'opera da imprimersi sopra le riproduzioni animali, Modena, Nella Stamperia di Giovanni Montanari, 1768. doi:https://doi.org/10.5962/bhl.title.158642.

[2] P. Freitas, A. Yandulskaya, J. Monaghan, Spinal cord regeneration in amphibians: A historical perspective 79 (2019) 437–452. doi:10.1002/dneu.22669.

[3] A. Tazaki, E. M. Tanaka, J.-F. Fei, Salamander spinal cord regeneration: The ultimate positive control in vertebrate spinal cord regeneration, Developmental Biology 432 (1) (2017) 63–71. doi:https://doi.org/10.1016/j.ydbio.2017.09.034.

[4] E. Chernoff, D. Stocum, H. Nye, J. Cameron, Urodele spinal cord regeneration and related processes, Dev Dyn (226) (2003) 295–307. doi:10.1002/dvdy.10240.

[5] A. Rodrigo Albors, A. Tazaki, F. Rost, S. Nowoshilow, O. Chara, E. M. Tanaka, Planar cell polarity-mediated induction of neural stem cell expansion during axolotl spinal cord regeneration, eLife 4 (2015) e10230. doi:10.7554/eLife.10230.
URL https://doi.org/10.7554/eLife.10230

[6] F. Rost, A. Rodrigo Albors, V. Mazurov, L. Brusch, A. Deutsch, E. M. Tanaka, O. Chara, Accelerated cell divisions drive the outgrowth of the regenerating spinal cord in axolotls, eLife 5 (2016) e20357. doi:10.7554/eLife.20357.
URL https://doi.org/10.7554/eLife.20357

[7] E. Cura Costa, L. Otsuki, A. Rodrigo Albors, E. M. Tanaka, O. Chara, Spatiotemporal control of cell cycle acceleration during axolotl spinal cord regeneration, eLife 10 (2021) e55665. doi:10.7554/eLife.55665.
URL https://doi.org/10.7554/eLife.55665

[8] S. Kondo, T. Miura, Reaction-diffusion model as a framework for understanding biological pattern formation, Science 329 (5999) (2010) 1616–1620. doi:10.1126/science.1179047.

[9] L. Seirin, E. Gaffney, R. Baker, The dynamics of turing patterns for morphogen-regulated growing domains with cellular response delays, Bull. Math. Biol. 73 (2011) 2527–2551. doi:https://doi.org/10.1007/s11538-011-9634-8.

[10] S. Y. Shvartsman, R. E. Baker, Mathematical models of morphogen gradients and their effects on gene expression, WIREs Developmental Biology 1 (5) (2012) 715–730. arXiv:https://wires.onlinelibrary.wiley.com/doi/pdf/10.1002/wdev.55, doi:https://doi.org/10.1002/wdev.55.
URL https://wires.onlinelibrary.wiley.com/doi/abs/10.1002/wdev.55

[11] R. Baker, P. Maini, Travelling gradients in interacting morphogen systems, Mathematical Biosciences 209 (1) (2007) 30–50. doi:https://doi.org/10.1016/j.mbs.2007.01.006.
URL https://www.sciencedirect.com/science/article/pii/S0025556407000107

[12] O. Chara, E. M. Tanaka, L. Brusch, Chapter ten - mathematical modeling of regenerative processes, in: B. Galliot (Ed.), Mechanisms of Regeneration, Vol. 108 of Current Topics in Developmental Biology, Academic Press, 2014, pp. 283–317. doi:https://doi.org/10.1016/B978-0-12-391498-9.00011-5.

[13] P. K. Maini, Mathematical models in morphogenesis, Springer Berlin Heidelberg, Berlin, Heidelberg, 1999, pp. 151–189. doi:10.1007/BFb0092377.
URL https://doi.org/10.1007/BFb0092377

[14] O. Wartlick, A. Kicheva, M. González-Gaitán, Morphogen gradient formation, Cold Spring Harb Perspect Biol.] 1 (3) (2009) a001255. doi:10.1101/cshperspect.a001255.

[15] J. Monaghan, Smoothed particle hydrodynamics and its diverse applications, Annual Review of Fluid Mechanics 44 (2012) 323–346. doi:http://dx.doi.org/10.1146/annurev-fluid-120710-101220.

[16] P. Degond, F.-J. Mustieles, A deterministic approximation of diffusion equations using particles, SIAM Journal on Scientific and Statistical Computing 11 (2) (1990) 293–310. doi:10.1137/0911018.

[17] A. S. Ceccarelli, A. Borges, O. Chara, Size matters: tissue size as a marker for a transition between reaction–diffusion regimes in spatio-temporal distribution of morphogens, Royal Society Open Science 9 (1) (2022) 211112. doi:10.1098/rsos.211112.

[18] J.-F. Fei, M. Schuez, A. Tazaki, Y. Taniguchi, K. Roensch, E. M. Tanaka, Crispr-mediated genomic deletion of sox2 in the axolotl shows a requirement in spinal cord neural stem cell amplification during tail regeneration, Stem Cell Reports 3 (3) (2014) 444–459. doi:https://doi.org/10.1016/j.stemcr.2014.06.018.

[19] E. M. Tanaka, Regeneration: If they can do it, why can't we?, Cell 113 (5) (2003) 559–562. doi:https://doi.org/10.1016/S0092-8674(03)00395-7.
URL https://www.sciencedirect.com/science/article/pii/S0092867403003957

[20] O. Wartlick, P. Mumcu, A. Kicheva, T. Bittig, C. Seum, F. Jülicher, M. González-Gaitán, Dynamics of dpp signaling and proliferation control, Science 331 (6021) (2011) 1154–1159. doi:10.1126/science.1200037.

[21] P. Müller, K. W. Rogers, B. M. Jordan, J. S. Lee, D. Robson, S. Ramanathan, A. F. Schier, Differential diffusivity of nodal and lefty underlies a reaction-diffusion patterning system, Science 336 (6082) (2012) 721–724. doi:10.1126/science.1221920.

[22] F. Michon, L. Forest, E. Collomb, J. Demongeot, D. Dhouailly, BMP2 and BMP7 play antagonistic roles in feather induction, Development 135 (16) (2008) 2797–2805. doi:10.1242/dev.018341.

[23] L. G. Morelli, K. Uriu, S. Ares, A. C. Oates, Computational approaches to developmental patterning, Science 336 (6078) (2012) 187–191. doi:10.1126/science.1215478.

[24] A. P. Pomreinke, G. H. Soh, K. W. Rogers, J. K. Bergmann, A. J. Bläßle, P. Müller, Dynamics of bmp signaling and distribution during zebrafish dorsal-ventral patterning 6 (2017) e25861. doi:10.7554/eLife.25861.

[25] A. Shellard, R. Mayor, Sculpting with stiffness: rigidity as a regulator of morphogenesis, Biochemical Society transactions 51 (04 2023). doi:10.1042/BST20220826.

[26] A. Mongera, P. Rowghanian, H. Gustafson, E. Shelton, D. Kealhofer, K. E. Carn, F. Serwane, A. Lucio, O. Giammona, J. andCampàs, A fluid-to-solid jamming transition underlies vertebrate body axis elongation, Nature 561 (2018) 401–405. doi:https://doi.org/10.1038/s41586-018-0479-2.

[27] N. I. Petridou, B. Corominas-Murtra, C.-P. Heisenberg, E. Hannezo, Rigidity percolation uncovers a structural basis for embryonic tissue phase transitions, Cell 184 (7) (2021) 1914–1928.e19. doi:https://doi.org/10.1016/j.cell.2021.02.017.
URL https://www.sciencedirect.com/science/article/pii/S0092867421001677

[28] H. I. Harn, S. P. Wang, Y. C. Lai, B. Van Handel, Y. C. Liang, S. Tsai, I. M. Schiessl, A. Sarkar, H. Xi, M. Hughes, S. Kaemmer, M. J. Tang, J. Peti-Peterdi, A. D. Pyle, T. E. Woolley, D. Evseenko, T. X. Jiang, C. M. Chuong, Symmetry breaking of tissue mechanics in wound induced hair follicle regeneration of laboratory and spiny mice, Nature communications 12 (1) (2021) 2595. doi:https://doi.org/10.1038/s41467-021-22822-9.

[29] G. Oster, J. Murray, H. AK, Mechanical aspects of mesenchymal morphogenesis, J Embryol Exp Morphol 78 (1983) 83–125.

[30] A. Gierer, H. Meinhardt, A theory of biological pattern formation, Kybernetik 12 (1972) 30–39. doi:https://doi.org/10.1007/BF00289234.

[31] A. M. Turing, The chemical basis of morphogenesis, Philosophical Transactions of the Royal Society of London. Series B, Biological Sciences 237 (641) (1952) 37–72. doi:10.1098/rstb.1952.0012.

[32] S. Motsch, D. Peurichard, From short-range repulsion to hele-shaw problem in a model of tumor growth, J. Math. Biol. 76 (2018) 205–234. doi:https://doi.org/10.1007/s00285-017-1143-4.

[33] J. Barré, P. Degond, E. Zatorska, Kinetic theory of particle interactions mediated by dynamical networks, Multiscale Modeling & Simulation 15 (3) (2017) 1294–1323. doi:10.1137/16M1085310.

[34] J. Barré, P. Degond, D. Peurichard, E. Zatorska, Modelling pattern formation through differential repulsion, Networks and Heterogeneous Media 15 (3) (2020) 307–352. doi:10.3934/nhm.2020021.